

Predicting air pressure in drainage stack of high-rise building*

E. S. W. WONG¹, Ying-lin LI (李应林)², Zuo-jin ZHU (朱祚金)^{1,2}

(1. Industrial Center, The Hong Kong Polytechnic University, Kowloon,
Hung Hom, Hong Kong, P. R. China;

2. School of Engineering Science, University of Science and Technology of China,
Hefei 230026, P. R. China)

Abstract It is necessary to understand the features of air pressure in a drainage stack of a high-rise building for properly designing and operating a drainage system. This paper presents a mathematical model for predicting the stack performance. A step function is used to describe the effect of the air entrainment caused by the water discharged from branch pipes. An additional source term is introduced to reflect the gas-liquid interphase interaction (GLII) and stack base effect. The drainage stack is divided into upper and base parts. The air pressure in the upper part is predicted by a total variation diminishing (TVD) scheme, while in the base part, it is predicted by a characteristic line method (CLM). The predicted results are compared with the data measured in a real-scale high-rise test building. It is found that the additional source term in the present model is effective. It intensively influences the air pressure distribution in the stack. The air pressure is also sensitive to the velocity-adjusting parameter (VAP), the branch pipe air entrainment, and the conditions on the stack bottom.

Key words air pressure in drainage stack, characteristic line method, stack base effect, interphase interaction

Chinese Library Classification O354

2010 Mathematics Subject Classification 76F02, 76G25, 65Z99

Nomenclature

a_1, a_2 , two eigenvalues;	\mathbf{F} , general flux vector in Eq. (10);
A_b , branch pipe water flow area;	f_1 , x -dependent parameter given by Eq. (4);
A_b' , branch pipe air flow area;	k_s , stack wall roughness (mm);
b_0 , time-averaged bottom pressure (Pa);	H_1 , stack base height (m);
b_1 , magnitude of the bottom pressure fluctuation (Pa);	H , stack height (m);
c_0 , sound speed under ambient condition (m/s);	L_x , length of the grid-step (m);
D, D_b , stack and branch pipe diameters (mm);	N_f , number of floors;
	p_0 , ambient air pressure (Pa);
	P_{av} , time-averaged pressure (Pa);

* Received Sept. 30, 2011 / Revised Sept. 25, 2012

Project supported by the National Natural Science Foundation of China (No. 10972212)

Corresponding author Zuo-jin ZHU, Associate Professor, Ph. D., E-mail: zuojin@ustc.edu.cn

P_{\min}	minimum peak pressure (Pa);	V_t ,	terminal speed given by Eq. (6) (m/s);
P_{\max}	maximum peak pressure (Pa);	v_k ,	speed of entrained air due to branch water discharged at x_k (m/s);
Pr ,	Prandtl number;	x ,	coordinate;
q ,	stack air flow flux ($\text{kg} \cdot \text{m}^{-2} \cdot \text{s}^{-1}$);	β ,	water injection angle;
q_w ,	water discharged from a branch pipe at x_k (l/s);	Δt ,	time step;
Q_w ,	stack water flow rate (l/s);	ϕ ,	phase angle;
S ,	step function of $(x - x_k)$;	γ ,	ratio of specific heat at constant pressure to that at constant volume;
\mathbf{S} ,	general vector of the source term in Eq. (10);	λ ,	ratio of temporal-spatio steps;
t_c ,	thickness of the annular water flow (mm);	σ_0 ,	velocity-adjusting parameter (VAP);
t ,	time;	σ_p ,	root mean square value of pressure (Pa);
\mathbf{u} ,	general variable vector in Eq. (10);	ρ_0 ,	ambient air density (kg/m^3);
v_{bg} ,	branch air speed (m/s);	θ ,	angle used to define A'_b in Eq. (8);
v_{bw} ,	branch water speed (m/s);	ϖ ,	coefficient of the viscous term in Eq. (23).
v ,	total entrained air speed (m/s);		

1 Introduction

The air pressure in a building drainage stack is generally dynamic as occurred in the stack of the Li Ka-shing building at Polytechnic University of Hong Kong^[1], there exists dynamically unsteady air entrainment caused by branch pipe water discharging, gas-liquid interphase interaction, and stack base effect^[2]. A larger positive air pressure in the stack can possibly deplete the trap seal, and then the contaminated air in the stack can leak into the space of buildings^[3]. This is evidently harmful to the occupants in a building. Hence, the features of the air pressure in a drainage stack need to be fully understood to prevent the contaminated air from leaking.

The previous numerical studies are based on the solution to the St Venant equations^[4-5], which emphasized the importance of the trap seal retention for improving the building operation^[6-11]. It has been found that the depletions of the trap seals^[3] and the bathroom floor drain traps^[12] can cause cross-contamination via the drainage system.

Zhang and Chen^[13] investigated the sanitary performance in a drainage stack and the related impact features. They measured the pressure oscillation limits and the permitted rate of the discharge water in a real-scale high-rise test building. The so-called permitted rate is defined according to the critical condition of whether the pressure oscillation limits have exceeded ± 400 Pa.

To predict the air pressure in a drainage stack of the high-rise building, a mathematical model is proposed, in which a step function is used to describe the influence of the entrained air flow from branch pipes, and an additional source term is introduced to reflect the gas-liquid interphase interaction (GLII) and stack base effect caused by the water impingement on the stack bottom wall.

The water discharge is a complicated fluid-flow process, in which the GLII and stack base effect is significant in impacting the stack air pressure. This indicates that the previous work^[4-5] did not consider the water discharge process in points of details. Nevertheless, in the view of applied mathematics and mechanics, the present mathematical model is just an extension of the St Venant equations.

Based on the present model, the governing equations of air flows in the stack region excluding the base region are solved by a total variation diminishing (TVD) scheme of the Yee-Roe-Davis type^[14-16], while those in the base part are solved by a characteristic line method (CLM). Recently, the TVD scheme was improved to analyze the gas-droplet detonation^[17] and to investigate shock-vortex interaction^[18], suggesting that this numerical scheme has more potential applications.

To show the model potential in engineering applications, the model parameters are calibrated

with the data measured by Zhang and Chen^[13]. The validation reveals the model parameters' sensitivity in predicting the air pressure in a drainage stack of a high-rise building.

The pressure evolution and distribution in the drainage stack are predicted by the present model. The effects of the air entrainment from branch pipes and the stack bottom condition can be ascertained more clearly from the point of fluid mechanics. The spatio-temporal evolutions of the velocity and pressure are presented and discussed.

2 Governing equations

Any small disturbance in air can propagate at a sound speed^[19], which is dependent on the air pressure and density. In a building drainage system, the small pressure disturbances caused by the discharged water, the gas-liquid phase interaction, and the stack base conditions can propagate in the stack air and lead to pressure fluctuations. The discharged water carries air from branch pipes into the stack, and causes the entrained air flow. The stack base effect leads to an increase in the mean air pressure and a decrease in the gas flow speed, and possibly causes a reverse gas flow in the base region. These air flow behaviors in the stack can be described by using the mass and momentum conservations.

Following Swaffield and Campbell^[4-5], for convenient modeling, it is assumed that the water flow in the vertical stack is annular, and the air flows in the stack core. The friction factor provides a viscous damping mechanism of the air flow when the air flow speed is larger than the terminal speed of the discharged water and an accelerating effect when the air flow speed is lower than the terminal speed. The discharged water can result in the air entrainment from the branch pipe into the stack.

By considering the air pressure in the stack as a one-dimensional unsteady variable and assuming that the pressure variation process is thermodynamically isentropic, the air pressure in the stack (p) can be represented by $p/\rho^\gamma \equiv \text{const.}$, where $\gamma = c_p/c_v = 1.4$ is the ratio of specific heat at constant pressure to that at constant volume, and ρ is the air density. Define the stack range by $x \in (0, H)$, where H is the stack height. Based on the conservation of mass and momentum of the stack air flow in a building drainage system, the governing equations of the air flow in the stack can be expressed as

$$\frac{\partial \rho}{\partial t} + \frac{\partial q}{\partial x} = 0, \quad (1)$$

$$\frac{\partial q}{\partial t} + \frac{\partial(q^2/\rho + p)}{\partial x} + \frac{4f}{2D} \frac{q^2}{\rho} + f_1 \rho v = 0, \quad (2)$$

and the mass flow rate is

$$q = \rho(u + v) = \rho \left(u + \sum_k v_k S(x - x_k) \right). \quad (3)$$

The water discharged from a branch pipe located at x_k results in a gas entrainment at a speed of $v_k(x_k)$. The step function $S(x - x_k)$ has a value of zero when $x < x_k$, and equals unity when $x \geq x_k$. It is used to reflect the effect of the discharged water, as seen in Fig. 1(a), with the total entrained air speed $v (= \sum_k v_k S(x - x_k))$. Different from the St Venant equations^[4-5], an

additional term with the parameter f_1 is introduced to consider the GLII and stack base effect. Assume that the top of stack is at $x = 0$ and the time step in simulation is Δt . Then, if the stack base has its relatively significant effect on the air motion when $x > H_1$, the x -dependent parameter f_1 may be expressed by

$$f_1 = \begin{cases} 0, & x \leq H_1, \\ -\frac{\sigma_0}{\Delta t} \frac{x - H_1}{H - H_1}, & \text{otherwise,} \end{cases} \quad (4)$$

where σ_0 is a velocity-adjusting parameter (VAP). (4) indicates that f_1 is assumed to be linear with the coordinate x . The larger σ_0 is, the more the intensive effect is, for the GLII and stack base. When $\sigma_0 = 0$, the form of the governing equations returns to the St Venant type.

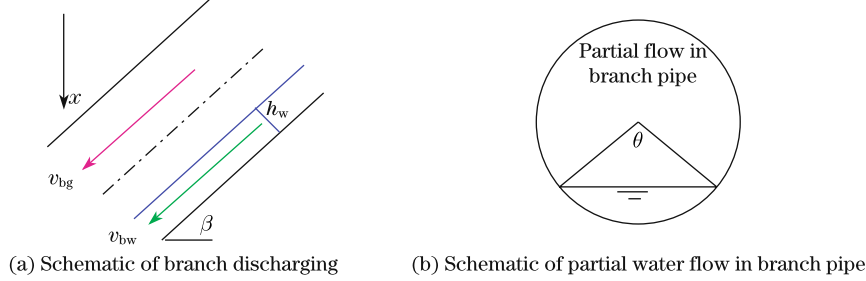


Fig. 1 Schematic of branch discharging and partial water flow in branch pipe

An example of the entrained air flow speed v as well as the terminal speed of the water flow V_t is given in Fig. 2. D represents the stack diameter. f denotes the friction factor of the air flow, which can be calculated by^[20]

$$f = 0.0303(k_s/t_c)^{1/3}, \quad (5)$$

where k_s is the stack wall roughness, and $t_c (= Q_w/(\pi DV_t))$ is the thickness of the annular water flow in which Q_w is the water flow rate and V_t is the terminal speed of water flow in the stack. The terminal speed can be calculated by^[20]

$$V_t = \frac{4.4034}{k_s^{0.1}}(Q_w/D)^{0.4}. \quad (6)$$

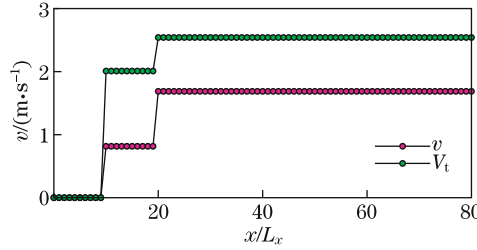


Fig. 2 Entrained air flow speed v and terminal speed V_t for $Q_w(x_1) = 2.5$ l/s and $Q_w(x_2) = 2$ l/s

Note that how to give the air entrainment from branch pipes accurately has not been ascertained to date since the air entrainment is related to the gas-liquid interface and the water flow speed in the branch. Hence, for the present simulation, we present a simple approximation. The branch water flow is partially fulfilled through a cross sectional area expressed as

$$A_b = \frac{D_b^2}{8}(\theta - \sin \theta). \quad (7)$$

As shown schematically in Fig. 1, the discharged water carries air from branch pipes into building stacks, leading to an air pressure drop at the corresponding locations connected to the branch pipe. The cross sectional area for the air flow in the branch pipe is given by

$$A'_b = \frac{D_b^2}{8}(2\pi - \theta + \sin \theta). \quad (8)$$

If the air speed v_{bg} in the branch can be assumed to be the same as the water speed v_{bw} (see Fig. 1(a)). Assume the flow rate of the water discharged from a branch pipe at x_k be $q_w(x_k)$, the speed v_k can be approximated by

$$v_k = 4(A'_b/A_b)q_w(x_k) \sin(\beta)/(\pi D^2). \quad (9)$$

The injection angle β is used together with the angle θ to determine the entrained air flow rate.

The initial air speed u and the relative air pressure in the stack are assumed to be zero. The intermediate height H_1 is used to partition a stack into the upper and base parts. The base part has a stagnation role on the air flow, leading to an increase in the mean air pressure in this part. The speed and pressure at the upper part are calculated by a total variation diminishing (TVD) scheme, while in the base part, they are calculated by a characteristic line method (CLM).

3 Numerical method

The air pressure in a building stack is usually calculated by solving the solutions to the St Venant equations with a characteristic line method^[4-11]. The previous studies have implicitly considered the air entrainment by imposing proper boundary conditions. However, the present governing equations (1) and (2) have explicitly reflected the influences of the water discharge and the GLII and stack base condition on the stack air pressure p . The mass balance of the gas flow in the stack is described in a conservative form.

To predict the air pressure in the upper part of the stack where the additional source term vanishes, the second-order symmetrical TVD method of a Yee-Roe-Davis type^[14-16] is used to solve the governing equations (1) and (2). This method was reported in detail by Shui^[21], and the applied to solve a two-phase traffic flow problem previously^[22]. The governing equations (1) and (2) can also be written in a general vector form as follows:

$$\frac{\partial \mathbf{u}}{\partial t} + \frac{\partial \mathbf{F}}{\partial x} + \mathbf{S} = 0, \quad (10)$$

in which

$$\mathbf{u} = (u_1, u_2)^T = (\rho, q)^T, \quad \mathbf{F} = (q, q^2/\rho + p)^T, \quad (11)$$

$$\mathbf{S} = (S_1, S_2)^T = \left(0, \frac{4f}{2D} \frac{q^2}{\rho}\right)^T, \quad (12)$$

where the superscript T denotes the matrix transposition. The corresponding Jacobian matrix

$$\mathbf{A} = \begin{pmatrix} a_{11} & a_{12} \\ a_{21} & a_{22} \end{pmatrix} = \begin{pmatrix} \frac{\partial F_1}{\partial u_1} & \frac{\partial F_1}{\partial u_2} \\ \frac{\partial F_2}{\partial u_1} & \frac{\partial F_2}{\partial u_2} \end{pmatrix} \quad (13)$$

has two eigenvalues

$$a_1 = \frac{1}{2}(a_{11} + a_{22} - \sqrt{(a_{11} - a_{22})^2 + 4a_{12}a_{21}}) = \frac{q}{\rho} - c, \quad (14)$$

$$a_2 = \frac{1}{2}(a_{11} + a_{22} + \sqrt{(a_{11} - a_{22})^2 + 4a_{12}a_{21}}) = \frac{q}{\rho} + c, \quad (15)$$

where $c = \sqrt{\frac{\partial p}{\partial \rho}}$ is the sound speed. Based on the two eigenvalues, there is the right eigen matrix

$$\mathbf{R} = (\mathbf{r}_1, \mathbf{r}_2) = \begin{pmatrix} r_{11} & r_{12} \\ r_{21} & r_{22} \end{pmatrix} = \begin{pmatrix} 1 & -\frac{a_{12}}{a_{11} - a_2} \\ -\frac{a_{21}}{a_{22} - a_1} & 1 \end{pmatrix}, \quad (16)$$

whose inverse represents the left eigen matrix

$$\mathbf{L} = \begin{pmatrix} \mathbf{l}_1 \\ \mathbf{l}_2 \end{pmatrix} = \mathbf{R}^{-1} = \frac{1}{1 - r_{12}r_{21}} \begin{pmatrix} 1 & -r_{12} \\ -r_{21} & 1 \end{pmatrix}. \quad (17)$$

The TVD method uses \mathbf{l}_k and \mathbf{r}_k to denote the left and right eigenvectors, which are, respectively, corresponding to the k -th eigenvalue of the matrix \mathbf{A} . Hence, the numerical flux at $x = x_{j+1/2}$ can be given by

$$\widehat{\mathbf{F}}_{j+1/2} = \frac{1}{2} \left(\mathbf{F}(\mathbf{u}_j) + \mathbf{F}(\mathbf{u}_{j+1}) + \sum_{k=1}^2 \psi_{k,j+1/2} \mathbf{r}_{k,j+1/2} \right), \quad (18)$$

$$\psi_{k,j+1/2} = -\frac{1}{\lambda} \left((\lambda a_{k,j+1/2})^2 g_{k,j+1/2} + (\varpi(\lambda a_{k,j+1/2})) (\alpha_{k,j+1/2} - g_{k,j+1/2}) \right), \quad (19)$$

$$\alpha_{k,j+1/2} = \mathbf{l}_{k,j+1/2} (\mathbf{u}_{j+1} - \mathbf{u}_j), \quad (20)$$

$$g_{k,j+1/2} = \min \text{mod}(\alpha_{k,j-1/2}, \alpha_{k,j+1/2}, \alpha_{k,j+3/2}), \quad (21)$$

where the ratio of the temporal-spatio steps is $\lambda = \Delta t/L_x$, and ϖ is the coefficient of the viscous term expressed as

$$\lambda = 0.988 / \max\{|a_{k,j+1/2}|\} \quad \text{for all } k, j, \quad (22)$$

$$\varpi(z) = \begin{cases} |z|, & z \geq \epsilon, \\ \frac{z^2 + \epsilon^2}{2\epsilon}, & \text{otherwise,} \end{cases} \quad (23)$$

where $\epsilon (= 0.025)$ is a small parameter used to define ϖ . The minimum modification function is given by

$$\min \text{mod}(z_1, z_2, z_3) = \begin{cases} \text{sgn}(z_1) \cdot \min(|z_1|, |z_2|, |z_3|), & \text{sgn}(z_1) = \text{sgn}(z_2) = \text{sgn}(z_3), \\ 0, & \text{otherwise,} \end{cases} \quad (24)$$

where $\text{sgn}(z)$ is a sign function whose value would be 1, 0, or -1 when z is positive, zero, or negative. The minmod function plays a role of monotonic treatment for the numerical solution, which can be calculated by the time step marching with

$$\mathbf{u}_j^{n+1} = \mathbf{u}_j^n - \lambda (\widehat{\mathbf{F}}_{j+1/2} - \widehat{\mathbf{F}}_{j-1/2}) - \frac{\Delta t}{2} (\mathbf{S}_{j+1} + \mathbf{S}_{j-1}). \quad (25)$$

According to the previous work^[11], the friction factor f in the source term (\mathbf{S}) is negative if the air flow speed (q/ρ) is less than the terminal speed (V_t) and positive when q/ρ is larger than V_t .

On the other hand, to predict the air pressure in the base part, the additional source term is needed, the characteristic line method (CLM) is used to solve the Euler-type equations, and then the CLM-based solutions are modified on the concept of time splitting.

In the base part of $x \in [H_1, H)$, at $x = x_j$, the solutions to the Euler-type equations are obtained by a characteristic line method

$$\begin{cases} \left(\frac{q}{\rho}\right)_j = (\zeta_1 + \zeta_2)_j/2, \\ (c)_j = (\zeta_1 - \zeta_2)_j(\gamma - 1)/4, \end{cases} \quad (26)$$

where c is the sound speed, and ζ_1 and ζ_2 are defined by

$$\zeta_1 = \frac{q}{\rho} + \frac{2c}{\gamma - 1}, \quad \zeta_2 = \frac{q}{\rho} - \frac{2c}{\gamma - 1}. \quad (27)$$

They are, respectively, the first and second invariances along the characteristic lines, i.e.,

$$\frac{dx}{dt} = \frac{q}{\rho} + c, \quad \frac{dx}{dt} = \frac{q}{\rho} - c. \quad (28)$$

The time splitting approach gives the following equations:

$$\begin{cases} \frac{\partial \rho}{\partial t} = 0, \\ \frac{\partial q}{\partial t} = -\frac{4f}{2D} \frac{q^2}{\rho} - f_1 \rho v \end{cases} \quad (29)$$

for the solution improvement. Assume that the ambient pressure and density are, respectively, p_0 and ρ_0 . Let $A = \sqrt{\gamma p_0 / \rho_0}$, $A_1 = 1 + \Delta t \frac{4f}{2D} \left(\frac{q}{\rho}\right)_j$. It is seen that

$$\begin{cases} \rho_j^{n+1} = \left(\frac{(c)_j}{A}\right)^{2/(\gamma-1)}, \\ q_j^{n+1} = \frac{1}{A_1} \left(\rho_j^{n+1} \left(\frac{q}{\rho}\right)_j - \Delta t (f_1 v)_j \frac{\rho_j^n + \rho_j^{n+1}}{2} \right), \end{cases} \quad (30)$$

where $(c)_j$ and $\left(\frac{q}{\rho}\right)_j$ are the CLM-based solutions to the Euler-type equations as given by (26).

The boundary conditions are given as follows. At $x = 0$, we assume

$$\rho(0) = \rho_0, \quad q(0) = 0. \quad (31)$$

At $x = H + L_x$, the relative pressure and mass flow rate can be expressed by

$$\begin{cases} P(H + L_x, t) = p - p_0 = b_0 + b_1 \cos(2\pi c_0 t / H + \phi), \\ q(H + L_x, t) = q(H, t), \end{cases} \quad (32)$$

where b_0 is the time-averaged bottom pressure, b_1 is the magnitude of the bottom pressure fluctuation, ϕ is the phase angle, and $c_0 (= \sqrt{\gamma p_0 / \rho_0})$ is the sound speed under the ambient condition. Then, using the CLM method, the values of ρ and q at $x = H$ can be predicted.

3.1 Calibration

As mentioned in the introduction section, the widely used St Venant equations^[4-5] can be considered as just a simpler model, which can be improved to extend its application potential.

The present model has further used artificial parameters, such as the velocity adjusting parameter which should be calibrated carefully. The TVD-CLM mixed method described in the previous section is used to predict the stack air pressure in a drainage system of the real-scale high-rise test building of 17 floors, where the flow rates of the water discharged from branch pipes are constants^[13].

It is noted that the real-scale high-rise test building for the experiments of Zhang and Chen^[13] is located in Shiga of Japan. The data recording work was done in 2006, in which the apparatus calibration is based on Japanese standard proposed by relevant engineering societies. The air pressure is measured by the pressure sensors in the type of VPRN-A3 of VELCOM. With the digital signal transmitter 9B02 of COLIN having a filter of 3 Hz, the collected pressure signals are recorded by the data logger OMNIACE-RT3424 of COLIN. The data logger has a measuring range of about ± 1000 Pa. The single floor height of the test building is around 2.8 m. The measured stack air pressure and its peak values^[13] are used to calibrate the model parameters, such as α_0 , β , b_0 , and b_1 , as shown in Fig. 3.

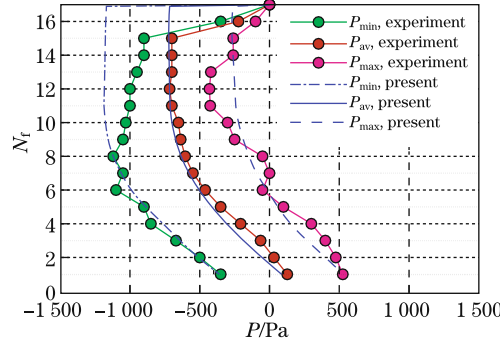


Fig. 3 Time-averaged pressure and its peak values plotted as functions of floor number N_f

The calibrated parameter values are

$$\begin{cases} p_0 = 1.0 \times 10^5 \text{ Pa}, & \rho_0 = 1.25 \text{ kg/m}^3, & \gamma = 1.4, & k_s = 1 \text{ mm}, \\ L_x = 0.28 \text{ m}, & D = D_b = 100 \text{ mm}, & x_1/L_x = 10, & x_2/L_x = 20, \\ q_w(x_1) = 2.5 \text{ l/s}, & q_w(x_2) = 2 \text{ l/s}, & \theta_1/\pi = 0.55, & \theta_2/\pi = 0.5, \\ b_0 = 100 \text{ Pa}, & b_1 = 450 \text{ Pa}, & \alpha/\pi = 1/9, & \sigma_0/\Delta t = 0.01, \\ \phi = 0, & H_1/L_x = 60, & H/L_x = 160, \end{cases} \quad (33)$$

where θ_k ($k = 1, 2$) are the discharging angles at x_k ($k = 1, 2$). It is noted that the value of H_1 is assigned according to the convenience of the numerical validation; the peak pressure values are expected to be $P_{av} \pm \sqrt{2}\alpha_p$, where P_{av} and α_p are, respectively, the time-average pressure and its root-mean square value because the approach of the peak value prediction is absolutely correct if the stack air pressure oscillates in a harmonic mode.

4 Results and discussion

To show the application potential of the developed mathematical model for the stack pressure prediction, using the TVD-CLM method and the parameters given in (33), we numerically explore the model parameters' sensitivity, and the evolution property of by velocity and pressure in the drainage stack.

4.1 Sensitivity to σ_0 , β , and b_1

The sensitivity of the numerical solutions to the three parameters VAP(σ_0), β , and b_1 is explored by comparing the distributions of the time-averaged relative pressure and the pressure peaks plotted as functions of the number of floor $N_f = 1 + (H - x)/(10L_x)$. The effect of VAP on the distributions of the peak pressures can be seen in Fig. 4, where other parameters have the same values as in (33). As seen in Fig. 4, VAP is a dominant parameter for the time-averaged

pressure distribution in the stack. The larger the value of VAP is, the smaller the pressure peak values are, indicating that VAP can be used as a key parameter in the calibration of the stack air pressure.

It is noted that the green curves in Fig. 4 are obtained on the basis of the traditional St Venant equations. From Fig. 4, it is clearly seen that whether the GLII and stack base effect has been considered properly, such as using VAP in the present model, is a key feature impacting the application potential of the model for the stack pressure prediction.

The distributions of peak pressures are also influenced by the branch entrainment, which depends on the β angle when the θ_k angle takes the values given in (33). Figure 5 shows that β significantly impacts the stack air pressure and its peaks. The suction pressure increases with the increase in β , indicating that the stack pressure is sensitive to the air entrainment from branch pipes.

The effect of the fluctuation magnitude of the bottom pressure b_1 on the time-averaged pressure and peak pressures can be seen in Fig. 6. The increase in the magnitude b_1 has no observable influence on the time-averaged pressure, but can enhance the root mean square value of the pressure fluctuation.

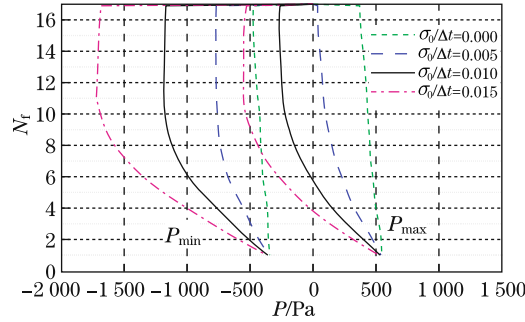


Fig. 4 Distributions of peak pressures along building height under different values of σ_0

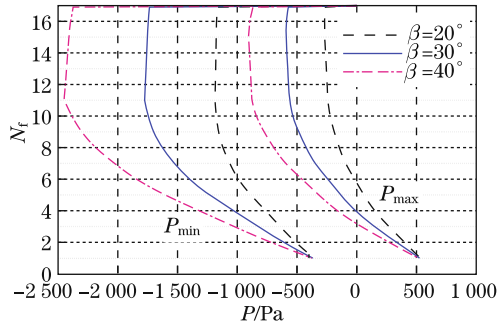


Fig. 5 Distributions of peak pressures along building height under different β

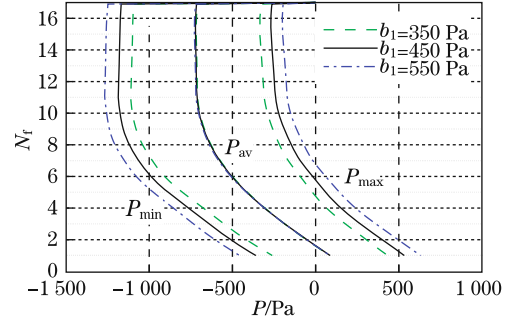


Fig. 6 Distributions of time-averaged pressure and its peak values along building height under different b_1

4.2 Evolutions of velocity and pressure

The distributions of the time-averaged peak pressures in the stack, as shown in Figs. 4–6, are related to the velocity and pressure evolutions in the stack. Using the parameters in (33), the simulation can output a temporal evolution of pressures at two stack locations, as illustrated in Fig. 7(a). For $t > 1$, the time-dependent pressure fluctuates approximately in harmonic and quasi periodic waves, while the time-average value and oscillation amplitude are evidently dependent on the stack location x/L_x . The time period of the pressure fluctuation is about H/c_0 .

Since the pressure oscillation is quasi-periodic, as shown in Fig. 3, the peak pressures can be approximated by multiplying the root mean square of the pressure fluctuation σ_p with a factor of $\sqrt{2}$ because $\frac{1}{2\pi} \int_0^{2\pi} (\sin \gamma)^2 d\gamma = \frac{1}{2}$.

Corresponding to the pressure fluctuation given in Fig. 7(a), the velocity fluctuation history in the time range of $t \in (1, 5)$ is shown in Fig. 7(b). According to the entrained speed v given in Fig. 2, with respect to the blue curve, the total velocity q/ρ at the stack bottom has a positive peak velocity of about 2.5 m/s. With respect to the black curve, at the location of $x = H_1$, the minimum value of q/ρ is close to 1 m/s. Approximately, harmonic and quasi-periodic fluctuating behaviors can also be found in the speed u -evolutions. Figure 7 also shows that the pressure peak corresponds to the u -velocity valley at a given location and vice-versa.

The contours of the pressure and velocity in the t - N_f plane are shown in Figs. 8–9. Due to the use of the calibrated parameter $\sigma = 0.01$, the air entrainment leads to the decrease in the stack air pressure $P(x, t)$, as shown in Fig. 8. The pressure is calculated by $(p - p_0)$, where the absolute pressure p is calculated by assuming that the gas flow is isentropic, i.e., $p/\rho^\gamma \equiv \text{const}$. The P -contours are labeled by -600 Pa, -300 Pa, 0 Pa, and 300 Pa, indicating that when $t > 1$ the stack air pressure P varies with time in a quasi-periodic mode due to the boundary conditions adopted. It is noted that the blue color region has the pressure less than -600 Pa, the cyan color region has the pressure in the range from -600 Pa to -300 Pa, the green color region has the pressure from -300 Pa to 0 Pa, the yellow color region has the pressure from 0 Pa to 300 Pa, the red color region has the pressure larger than 300 Pa. This spatio-temporal P -evolution indicates that the gas flow in the building stack is oscillating under the influences of the branch discharging, gas-liquid interphase interaction and the stack base.

Figure 9 illustrates the temporal-spatio evolution of $u(x, t)$ ($= q/\rho - v$). It is noted that the blue color region has a speed less than -0.5 m/s, the cyan color region has a speed in the range from -0.5 m/s to 0 m/s, the green color region has a speed from 0 m/s to 1 m/s, the yellow

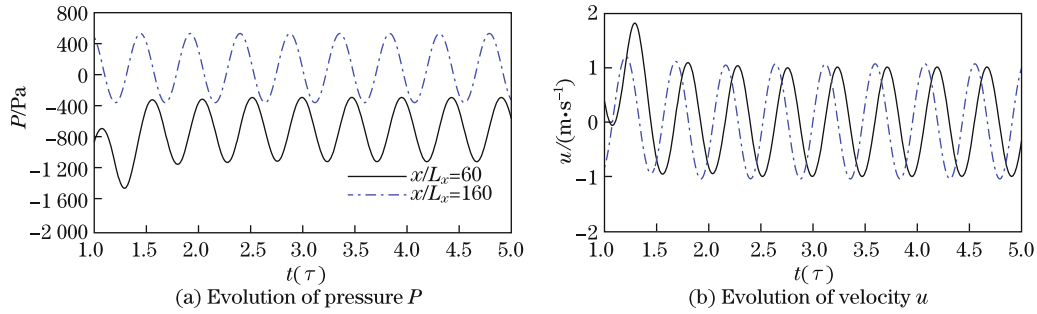


Fig. 7 Evolutions of pressure P and velocity u at $x/L_x = 60$ and 160

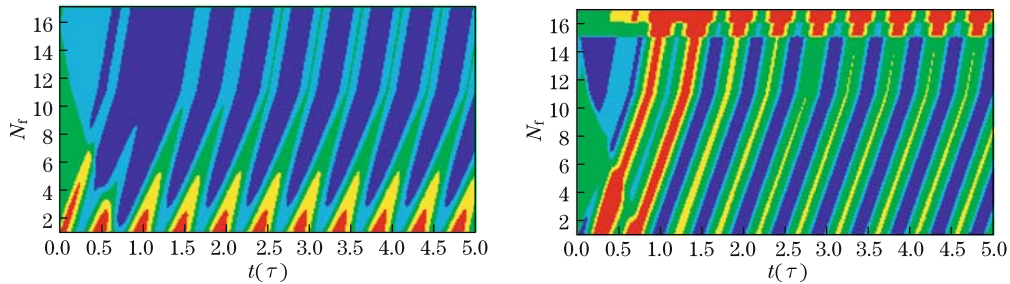


Fig. 8 Contours of stack pressure in t - N_f plane

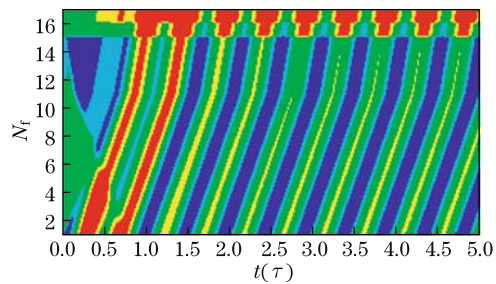


Fig. 9 Contours of $u(x, t)$ in t - N_f plane

color region has a speed from 1 m/s to 1.5 m/s, and the red color region has a speed larger than 1.5 m/s. The speed u-contours show that the velocity is generally positive on the floors when $N_f > 15$. However, when $N_f \leq 15$ and $t > 1$, it is oscillating around zero (m/s) and its value slightly depends on the stack location.

5 Conclusions

A model for predicting the stack air pressure in the drainage system of a high-rise building has been proposed. A step function is used to reflect the effect of the entrained air flow caused by the water discharged from branch pipes. An additional source term is introduced to take account of the GLII and stack base effect. The current model has a larger application potential. The governing equations are solved by a TVD-CLM mixed method applied to the upper and base parts of a stack. Four model parameters, i.e., σ_0 , β , b_0 , and b_1 , can be effectively calibrated by the experimental data in a real-scale high-rise test building. The sensitivity of the numerical results to the velocity adjusting parameter, the air entrainment from branch pipes, and the fluctuation magnitude of the bottom pressure are investigated. It is found that the velocity adjusting parameter σ_0 in the additional term plays a deterministic role on the distribution of the time-averaged stack air pressure. The magnitude of the bottom pressure fluctuation has an evident influence on the root mean square value of the stack air pressure.

Acknowledgements The work is partially supported from the Automation Unit in Polytechnic University of Hong Kong. We wish to acknowledge Dr. T. Y. CHEN in Polytechnic University of Hong Kong for his proofreading of the manuscript, and Senior Engineer Mrs. L. ZHANG in China National Engineering Research Center for Human Settlements for some helpful private communications. We also thank the anonymous referees' suggestions.

References

- [1] Wong, E. S. W., Chan, D. W. T., and Zhu, Z. J. Fluctuation behaviors of air pressure in a high-rise building drainage system. *Journal of Architectural Engineering*, **17**(2), 82–84 (2011)
- [2] Swaffield, J. A., Jack, L. B., and Campbell, D. P. Control and suppression of air pressure transients in building drainage and vent systems. *Building and Environment*, **39**(7), 783–794 (2004)
- [3] Kelly, D. A., Swaffield, J. A., Jack, L. B., Campbell, D. P., and Gormley, M. Pressure transient identification of depleted appliance trap seals: a pressure pulse technique. *Building Services Engineering Research and Technology*, **29**(2), 165–181 (2008)
- [4] Swaffield, J. A. and Campbell, D. P. Air pressure transient propagation in building drainage vent systems, an application of unsteady flow analysis. *Building and Environment*, **27**(3), 357–365 (1992)
- [5] Swaffield, J. A. and Campbell, D. P. Numerical modelling of air pressure transient propagation in building drainage vent systems, including the influence of mechanical boundary conditions. *Building and Environment*, **27**(3), 455–467 (1992)
- [6] Swaffield, J. A. and Campbell, D. P. The simulation of air pressure propagation in building drainage and vent systems. *Building and Environment*, **30**(1), 115–127 (1995)
- [7] Wright, G. B., Jack, L. B., and Swaffield, J. A. Investigation and numerical modeling of roof drainage system under extreme events. *Building and Environment*, **41**, 126–135 (2006)
- [8] Swaffield, J. A. Sealed building drainage and vent systems— an application of active air pressure transient control and suppression. *Building and Environment*, **41**, 1435–1446 (2006)
- [9] Swaffield, J. A. Simulation of building drainage flows, waste solid transport and vent system transients. *Building Services Engineering Research & Technology*, **17**(2), B4–B8 (1996)
- [10] McDougall, J. A. and Swaffield, J. A. Simulation of building drainage system operation under water conservation design criteria. *Building Services Engineering Research & Technology*, **21**(1), 41–51 (2000)

-
- [11] Swaffield, J. A. and Jack, L. B. Simulation and analysis of airborne cross-contamination routes due to the operation of building drainage and vent systems. *Building Research Information*, **32**(6), 451–467 (2004)
- [12] Gormley, M. Air pressure generation as a result of falling solids in building drainage stacks: definition, mechanisms and modelling. *Building Services Engineering Research and Technology*, **28**(1), 55–70 (2007)
- [13] Zhang, L., and Chen, Y. F. *Experimental Report on the Impact Features of Sanitary Performance in Drainage Stack Systems, Part II: Experimental Data* (in Chinese), Report of China National Engineering Research Center for Human Settlements, 78–92 (2006)
- [14] Yee, H. C. Construction of explicit and implicit symmetric TVD schemes and their applications. *J. Comput. Phys.*, **68**, 151–179 (1987)
- [15] Roe, P. C. Approximate Riemann solvers, parameter vectors, and difference schemes. *J. Comput. Phys.*, **43**, 357–372 (1981)
- [16] Davis, S. F. Simplified second-order Godunov-type methods. *J. Sci. Statist. Comput.*, **9**, 445–473 (1988)
- [17] Guo, Y. H., Tian, Z., and Hao, B. T. Implicit TVD schemes applied to gas-droplet detonation calculation. *Appl. Math. Mech. -Engl. Ed.*, **21**(6), 725–732 (2000) DOI 10.1007/BF024602192
- [18] Tu, G. H., Yuan, X. J., Xia, Z. Q., and Hu, Z. A class of compact upwind TVD difference scheme. *Appl. Math. Mech. -Engl. Ed.*, **27**(6), 765–772 (2006) DOI 10.1007/s10483-006-0607-1
- [19] Rottly R. M., *Introduction to Gas Dynamics*, John Wiley and Sons, New York, 42–59 (1962)
- [20] Jack, L. B. *An Investigation and Analysis of Air Pressure Regime Within Building Drainage Vent System*, Ph.D. dissertation, Heriot-Watt University, Edinburgh (1994)
- [21] Shui, H. S. *Finite Difference in One Dimensional Fluid Mechanics* (in Chinese), National Defense, Beijing, 343–551 (1998)
- [22] Zhu, Z. J. and Wu, T. Q. Two-phase fluids model for freeway traffic flow and its application to simulate evolution of solitons in traffic. *J. Transp. Engng.*, **129**(1), 51–56 (2003)